CHAPTER 8

Basic Cell–Cell and Cell–Surface Interactions in Liposome and Cellular Systems

Ulrike Gimsa,[1] Veronika Kralj-Iglič,[2] Aleš Iglič,[3] Stefan Fiedler,[4] Michael Zwanzig,[4] Ludwig Jonas,[5] and Jan Gimsa[6]

[1]*Research Institute for the Biology of Farm Animals, Germany*
[2]*Institute of Biophysics, Faculty of Medicine, University of Ljubljana, Slovenia*
[3]*Laboratory of Physics, Faculty of Electrical Engineering, University of Ljubljana, Slovenia*
[4]*Fraunhofer Institute Reliability and Microintegration (IZM), Berlin, Germany*
[5]*Electron Microscopy Center, University of Rostock, Germany*
[6]*Chair of Biophysics, Faculty of Biology, University of Rostock, Germany*

Contents

Abstract

Experimental evidence on long, thin tubular structures (with or without transport gondolas) in giant phospholipid vesicles indicates an important role of phospholipid nanotubes in intracellular and intercellular transport and communication. In this work, we present evidence that nanotubular structures similar to the ones observed in giant phospholipid vesicles exist also in fully differentiated cells.

We have used sub-micron metal-rod decorated surfaces, "nanolawn" structures, as a substrate to study cell–cell and cell–surface interactions of primary murine astrocytes. Astrocytes are the major cell group of the brain, comprising about 50% of the cells. They support neurons both physically as a cell matrix and physiologically by providing a stable microenvironment and growth factors. Astrocytes form multicellular syncytia *in vivo* that provide neuronal homeostasis by taking up neurotransmitters and buffering the ionic content of the extracellular medium in the brain. Using nanolawn as the matrix for differentiation, we could observe how astrocytes form nanotubular protrusions to make contact with the matrix and each other. The thin tubular structures were very similar to those in pure phospholipid systems. Furthermore, gondolas on these nanotubes have been observed suggesting a transport function for cellular material. It could be theoretically

ADVANCES IN PLANAR LIPID BILAYERS AND LIPOSOMES, VOLUME 5
ISSN 1554-4516 DOI: 10.1016/S1554-4516(06)05008-3

shown that curvature-induced self-assembly of interacting anisotropic membrane components may lead to the spontaneous formation of thin nanotubular membrane protrusions in systems of giant liposomes as well as in astrocytes. This self-assembly may represent a relevant physical mechanism of nanotube formation even if membrane skeleton elements, such as actin fibers, were not essential for the nanotube formation.

1. INTRODUCTION

Thin tubular structures are abundant in cellular systems. They have been called filopodia [1], tunneling nanotubules (TNTs) [2,3], cytonemes [4,5], tethers [6], or simply nanotubes [7]. They appear to have a broad range of functions. Filopodia have first been described in living cells by Gustafson and Wolpert [8]. They observed migration of mesenchymal cells at the interior wall of the blastocoelic cavern of sea urchins and got the impression that the filopodia produced by these cells explored the substrate. They assumed that filopodia were extended to gather spatial information – a notion supported by other authors as well [9,10]. Other functions ascribed to nanotubes extending from cells are the exchange of material or signalling molecules [2,11,12]. Nanotubes are even suspected to carry cell organelles such as mitochondria [13]. In addition, their formation is induced by intracellular bacteria, such as *Listeria monocytogenes*, using the tubes to travel from cell to cell [14,15].

Nanotubes play a role in various cell types. Here, we will discuss their role in the immune and the nervous system. We will show data on nanotubular protrusions with which astrocytes adhere to an artificial substrate, that is, sub-micron metal-rod decorated surfaces. Research on the cellular interaction with artificial substrates is motivated by the need for optimized biomaterials for cells to grow on, such as matrices for tissue regeneration [16] or materials where cells are intended to not grow upon, such as stents or heart valves [17].

Most of the observed cellular nanotubes employ actin filaments. However, nanotubular structures may also develop in cell-free systems [18,19]. Cellular exocytosis has been modelled in protein-free liposomes and has been shown to involve nanotube formation [20]. Furthermore, we will provide theoretical and practical evidence from our own laboratories that actin is not necessary for nanotube formation.

2. BIOLOGICAL RELEVANCE OF NANOTUBE FORMATION – LESSONS FROM OTHER LABORATORIES

2.1. Nanotubes in the immune system

The immune system's main functions are defense against invading pathogens and preventing cancer by destroying transformed cells. It is set up as a

complicated network of different cell types, both mobile and tissue resident. Therefore, intercellular communication is a prerequisite for optimal function. Recently, nanotubes have been discovered to functionally connect immune cells [12]. These nanotubes connect dendritic cells, the most potent antigen-presenting cells of the immune system. Following stimulation with bacterial products, dendritic cells transmit calcium fluxes over distances up to 100 μm. This transport is not mediated by gap junctions or by release of ATP. Both calcium fluxes and injected dye traces are transported through these connections, which have a length of up to 100 μm and an average diameter of 35 nm. While the authors observed between 0 and 75 nanotubes per cell in living cell samples, reduced numbers were seen in fixed samples where numerous discontinued fragments where found. The connections are transient in live cells. Time-lapse microscopy revealed that connections form and disappear frequently between cells over a period of several minutes [12]. Dendritic cells extend lamellipodia in response to stimulation with bacterial products [21]. Spreading of lamellipodia followed contact by nanotubes and calcium fluxes [12]. The tracing dye, Lucifer yellow, travels through these nanotubes to ~5–6 surrounding cells. Apparently, the open lumen of the nanotubes is limiting, as the bigger texas red dextran does not travel [12]. Interestingly, no calcium fluxes were observed in non-myeloid cells, for example, fibroblasts, although they were connected by nanotubes [12]. The authors assume that contact of antigen or inflammatory stimuli with dendritic cells might lead to a prompter response when cells are interconnected via nanotubes. Antigen processing might be faster and a local inflammatory response might occur more rapidly as if mediated by the secretion of cytokines [12]. It has been shown that dendritic cells underlying gut epithelial cells can project dendrites in between cells even through tight junctions in order to access bacteria in the gut lumen [22].

It has been shown that also most other immune cells such as B cells, T cells, NK cells, monocytes and neutrophils form nanotubes [7,23,24]. It is not known whether signaling via nanotubes is relevant to T-cell activation, as immune synapses require close opposition of membranes and a large interface [25]. It has been speculated however, that B cells upon stimulation of B-cell receptors extend nanotubes (here called cytonemes) on which they present antigens to search for rare T cells with the appropriate T-cell receptor [24]. These cytonemes reach a length of up to 80 μm and are 200–400 nm in thickness. They often show a branched structure with concentrated lipid-raft staining at the branching points. Otherwise, lipid-raft structures are punctately distributed along the cytoneme shafts and especially to be found at the tip of the cytoneme. Actin has been found distributed similarly along the shaft. The authors however do not report a colocalization and whether they found actin also at the tips of the cytonemes [24]. The time course of appearance of these cytonemes is consistent with early activation events and supports the hypothesis that these structures might be used for transport of signaling molecules or receptors. They show up as early as 5 min after B-cell receptor stimulation and grow and stabilize over 30–40 min. Their

growth rate is 0.2 μm/s [24]. Nanotubes in neutrophils have been assumed to increase the capacity for adhesion, catching and holding of objects for phagocytosis over a distance [26]. In another study, membrane nanotubes connecting cells have been shown for B cells, macrophages and NK cells [7]. The authors report "bulges" travelling along the nanotubes comparable to gondolas described by Rustom *et al.* [2]. The nanotubes indeed transport cellular material as the authors show that lipids from two cells can mix. Thus, they assume that the nanotubes also provide a mechanism for the intercellular transfer of cell surface proteins [7]. In addition to nanotube formation from actin-driven protrusions, described by Rustom *et al.* [2], they found nanotube formation between cells that were previously connected via an immunological synapse as cells separated [7].

2.2. Nanotubes in the central nervous system

Nanotubes in the central nervous system (CNS) have been observed on neurons and astrocytes. Zhou and Cohan [27] showed that actin filaments determine structure and motility of neuronal growth cones. Microtubules support growth-cone-mediated axon extension. Actin filaments project radially throughout the growth cone into filopodia. Microtubules project from the axon shaft to the central region of the growth cone in a bundled form. Apparently, both actin and microtubules are necessary for growth-cone extension [27].

While connectivity between neurons obviously serves electrical signalling between neurons, thus transmission of information, connections of astrocytes to astrocytes or neurons fulfill other tasks. Astrocytes comprise about 50% of the cells of the brain. They support neurons both physically as a cellular matrix and physiologically by providing stable microenvironment and growth factors. Astrocytes form multicellular syncytia *in vivo* that ensure neuronal homeostasis by taking up excess neurotransmitters (e.g., glutamate) and buffering the ionic content of the extracellular medium in the brain [28,29]. They enwrap dendritic spines or whole synapses of neurons [30,31] and show a high motility of their processes at active neuronal synapses [32]. Hirrlinger *et al.* [32] show motility of astrocytes *in situ*, that is, in living brain slices. They show extension of membrane tubes of < 1 μm in diameter and 2–6 μm in length. Their extension process lasts for 30–90 s. The majority of these filopodia stayed transiently elongated for 3–6 min, while the minority stayed for longer than 15 min. How this motility is achieved has not been resolved yet. The physiological function of this intimate contact is probably to position signalling molecules directly to the sites of neurotransmission and to modulate neuronal communication [32]. Astroglial membranes contain numerous neurotransmitter receptors and transporters, and are thus equipped to sense and regulate formation, stability and efficacy of synapses [33,34]. Astrocytes of the hippocampal formation show a surface density of glutamate transporters on their membranes of about 10,800/μm^2 [35].

As mentioned earlier, one of the functions of astrocytes is to take up excess glutamate. Nevertheless, Ventura and Harris [31] found that only 57% of the synapses had astrocytes surrounding them. The authors assume that astrocytes extend filopodia towards active glutamate-releasing synapses.

2.3. Artificial substrates

Tissue regeneration is one of the hypes and hopes of contemporary biomaterials research. Efficient and undisturbed growth of cells on implants is a requirement for bone regeneration [16,36] or artifical joints [37]. Other applications are, for instance electrode arrays on which electrically active cells such as neurons, are grown and their activity is observed (see later). Here, not only materials but also their surface properties play an important role. It has been shown that smooth muscle cells of bladder adhere best to nanostructured surfaces. This makes sense as the extracellular matrix encountered by cells *in vivo* represents such a nanostructured surface. An astroglial cell line has been grown on smooth silicon and arrays of silicon pillars and wells [38]. These cells preferred the pillar substrates to the smooth surface. While growing on pillars, cells did not sag down onto the smooth-etched surface. The authors assume that the cytoskeleton or other mechanical effects might be responsible for this phenomenon. Alternatively, the greater availability of nutrients from the medium when cells stayed elevated on pillar tops or an aversion of the smooth silicon floor might have played a role.

In this chapter, we demonstrate how primary murine astrocytes grow on submicron metal-rod decorated surfaces, so-called "nanolawns". Because of their special abilities of connecting cells in the brain, astrocytes make up an ideal model system for investigating the interaction of cells with nanostructured surfaces. Our main focus was on how the cells interact with the non-living material, how they form membrane protrusions and how cellular material – making up these protrusions and finally constituting a confluent cell layer – is transported. To that end, we used histological staining combined with fluorescence microscopy and scanning (SEM) as well as transmission electron microscopic imaging (TEM).

3. NANOTUBES IN CELLULAR AND PHOSPHOLIPID SYSTEMS *IN VITRO* – DATA AND THEORIES FROM OUR LABORATORIES

3.1. Neuronal networks on chips

Multielectrode arrays can be used to detect electric activity in neuronal networks (Fig. 1). For this, primary neuronal cell cultures, which are actually astrocyte-neuron co-cultures, were prepared from neonatal mouse cortices and grown on

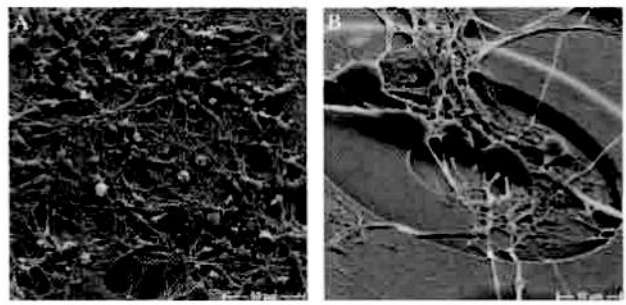

Fig. 1. Astrocyte-neuron co-culture on neuro-cell chips. (A) Overview of cells on a silicon chip with four signal pick up electrodes. (B) Neurons and astrocytes of a neuronal network are highly interconnected.

the surface of silicon chips, that is, artificial substrates [39]. From their appearance, astrocytes and neurons can hardly be distinguished.

3.2. Astrocytes on nanostructured surfaces

Sub-micron metal rod decorated metal foils (metal nanolawn) have been prepared according to Schönenberger *et al.* [40] using commercially available nucleopore filters, that is, chemically etched polycarbonate ion-track membranes (Millipore, 0.6 μm pores, Schwalbach, Germany) as template. Briefly, poly-carbonate filter membranes have been coated by gold sputtering at one side to obtain a conductive metal layer. This layer has been further enhanced up to ~10 μm thickness in a fine gold- or platinum-plating bath (Auruna 591 and Platin K; Umicore Galvanotechnik GmbH, Schwäbisch-Gmünd, Germany). The polymer pores have been galvanically filled by cathodic deposition of up to 3 μm. The polymer template has subsequently been removed in boiling dichloromethane. The resulting metal foils have been washed twice, dried and cut. Substrate pieces of $3 \times 2\,mm^2$ have been sterilized in 70% aqueous ethanol prior to cell-culture setup.

Each metal pillar has a diameter of ~600 nm (Fig. 2). The density of the pillars on the foil is $3.6 \times 10^{11}\,m^{-2}$. Vertical pillars of platinum nanolawn are around 1.6 μm long and planar at the top. The gold pillars are longer (around 2.6 μm) with tips of varying edgy shapes, depending on the crystal structure at the tip. About 37% of the pillars are vertically oriented. The others are tilted at different angles.

Primary cortical astrocytes were isolated from neonatal mice as described before [41]. Briefly, the frontal cortex was isolated from the brain, pools prepared and then mechanically dissociated through a nylon membrane. The cells were seeded onto poly-L-lysine (10 μg/ml in H_2O; Sigma-Aldrich, Taufkirchen, Germany)-coated plastic dishes. Astrocytes reached confluency after 10 days. They were detached by Accutase (PAA, Cölbe, Germany) treatment and seeded onto poly-L-lysin-coated nanolawn structures.

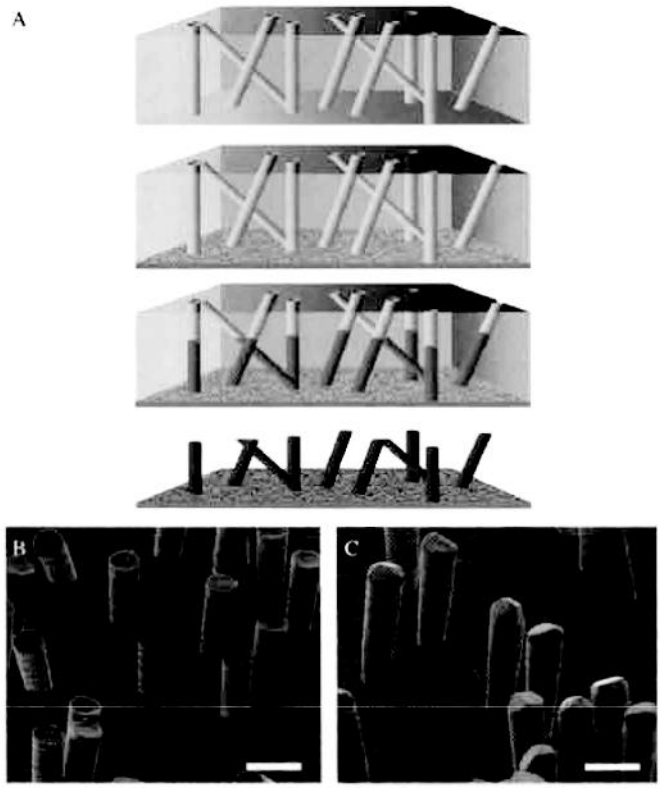

Fig. 2. Sub-micron metal rod decorated surfaces that is, nanolawn. (A) Production of nanolawn on isoporous track-etched polymer template. Polymer membranes are coated by gold sputtering. This layer is enhanced in a platinum or gold plating bath. Polymer pores get filled by cathodic deposition. Polymer template gets removed. Depending on metal-plating conditions, multicrystalline pillars with different grain size can be produced. (B) Platinum nanolawn. (C) Gold nanolawn. Scale bars of SEM images in B and C represent 1 μm.

The cells accepted these unusual culture substrates equally without any problems, and their morphology was very similar on glass slides (Fig. 3A1) and nanolawns (Fig. 3B1 and C1). We found very little dead cells after 72 h as detected by propidium iodide staining (Fig. 3A2, B2 and C2). This is in line with previous observations of astrocytes growing on silicon pillar arrays [38].

Our astrocytes formed contacts to the metal pillars within minutes (Fig. 4A). Indeed, the formation of nanotubes could have been much more rapid than that, because 10 min was the shortest time interval we examined. As described earlier, the formation of astrocyte filopodia-like processes has been observed within seconds [32]. Moreover, these filopodia retracted again within minutes, a process which we could not observe because our cultures had been fixed before analysis. In our cultures, astrocytes extended nanotubes of ~100 nm in diameter to neighbouring metal pillars and from there to further pillars while maintaining contact to

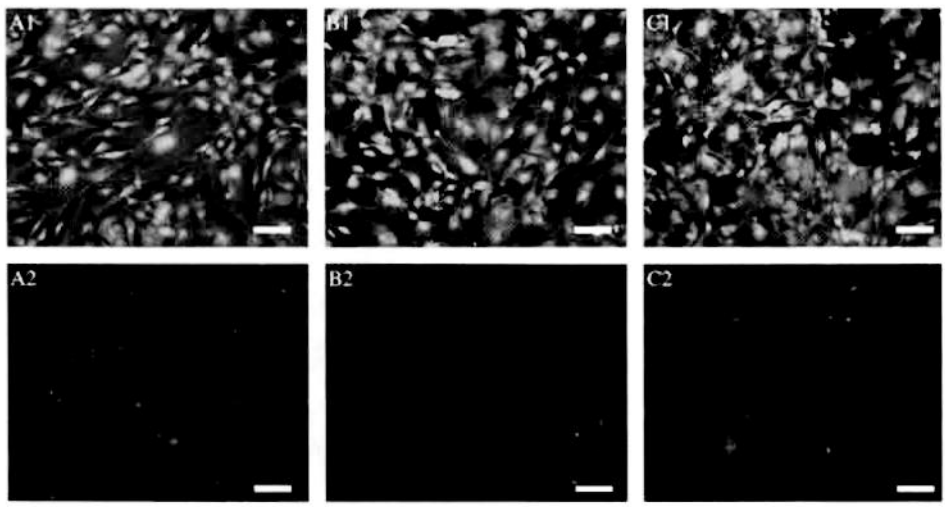

Fig. 3. Primary murine astrocytes after 72 h on poly-L-lysin-coated glass slides. (A) Gold (B) Platinum (C) Nanolawns. Astrocytes were stained intracellularly with CFSE (A1-C1) or propidium iodide (A2-C2) which revealed uncompromised growth and negligible cell death on nanolawns. Scale bars = 100 μm (for color version: see Color Section on page 423).

pillars that had been reached before (Fig. 4B). The tubes extend over several micrometers at a roughly constant diameter (Fig. 4C) but may develop into very long tubes (> 100 μm) at a larger diameter (still < 1 μm) (Fig. 4D). From our observations it could be assumed that astrocytes aimed at growing to confluency by making contact to cells further away (Fig. 4D).

The nanotubes appear straight when directly connecting two attachment points on metal pillars (Fig. 5B) while their correspondent structures grown on poly-L-lysin-coated glass surfaces (Fig. 5A) displayed serpentine shapes. Apparently, the material necessary to prolong them was transported along the nanotubes in gondola-like structures (Fig. 5B, arrows). That gondolas are indeed transport vehicles and not leftovers of broken connections to metal pillars is supported by our observation of gondola-like structures as early as 10 min of culture when nanotubular extensions start the process of monolayer formation on nanolawns from cells which are spherical and singularized at the moment of seeding (Fig. 6A). Gondolas can be found in varying frequency. Sometimes, many gondolas are carried by one nanotube (Fig. 6B). Nanotubes may branch into two continuing nanotubes (Fig. 6B). The angle between an attached nanotube and the continuative tube is in the range of 90–180 degree.

Most nanotubes do not display any gondolas at the time of fixation. This might be explained by rapid formation and transport of these structures. Gondolas between two connected macrophages have been shown to form within seconds and move for a period of 160 s with a constant speed of 0.16 μm/s [7]. While Rustom *et al.* [2] showed that nanotubes formed *de novo* by actin-driven

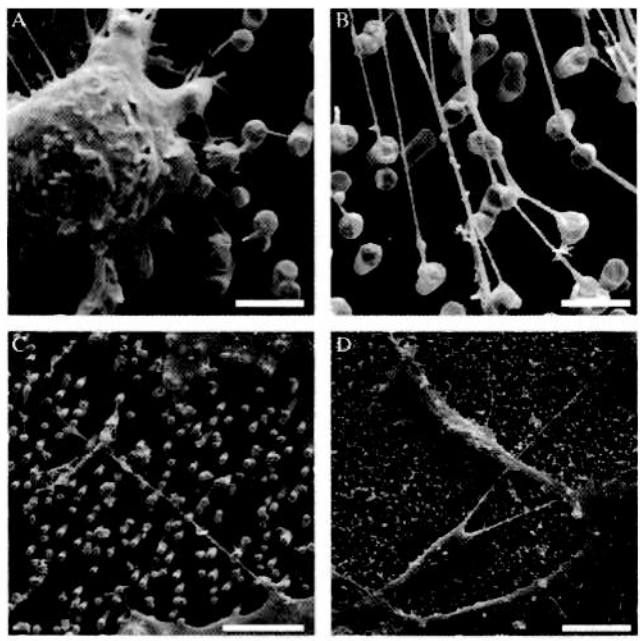

Fig. 4. Astrocytes growing on nanolawns (SEM images). (A) Astrocytes make contact to metal pillars via nanotubular membrane protrusions within 10 min. They extend nanotubes of about 100 nm in diameter to distant metal pillars via neighbouring pillars while maintaining contact to pillars that were reached before; (B) Nanotubes may extend over several micrometers at this diameter; (C) But may develop into very long tubes ($>100\,\mu m$) at a higher diameter which is still $<1\,\mu m$. (D) Astrocytes presumably aim at growing to confluency by making contact to cells further away. Scale bars in A, B, C and D represent 2, 2, 8 and 20 μm, respectively.

membrane protrusions extending from one cell to another, Önfelt *et al.* [7] demonstrated that nanotubes may also arise from cells that have been connected via an immunological synapse and move apart. These nanotubes might be formed by an alternative mechanism starting from membrane bridges. The latter authors also showed that branched nanotubes may connect three cells to form a network. They observed that when a branch to one cell broke, the remaining two cells stayed connected and assumed that this effect required some contraction of the tube. Önfelt *et al.* [7] hypothesized that the nanotubes are constructed with fluid membrane that can flow easily between the nanotubes and the cell surface.

Transmission electron micrographs showed that cell bodies and nuclei sagged between metal pillars (Fig. 7A) while nanotubular protrusions seem to be restricted to the upper parts of the pillars (Fig. 7B). When observed from an angle, it became clear that this also applied to the peripheral membrane surfaces (Fig. 7B). Hirrlinger *et al.* [32] described that the astrocytic somata stayed stationary. This corresponds to our finding that somata with nuclei are found in

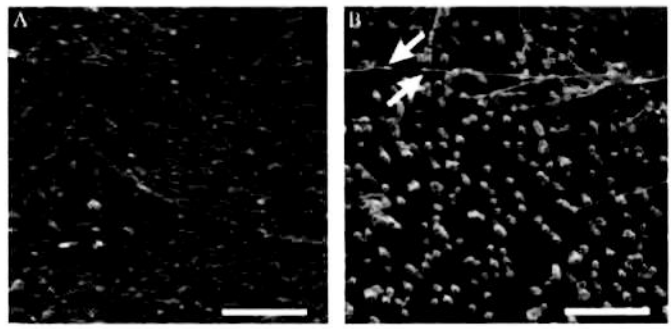

Fig. 5. (A,B). Nanotubes appear straightened in between two attachment points on metal pillars (B) while their correspondent structures grown on poly-L-lysin coated glass surfaces are randomly coiled (A). Arrows point at gondola-like structures (B). Scale bars in A and B represent 8 μm.

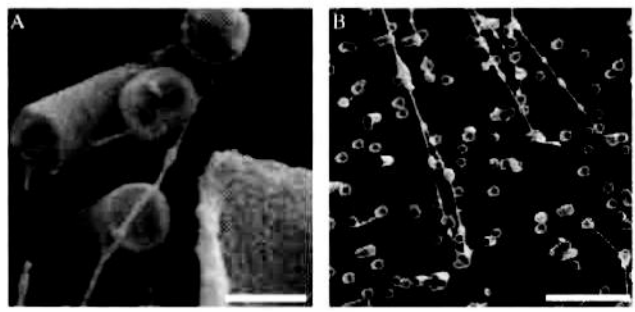

Fig. 6. Apparently, the material necessary to prolong the nanotubes was transported along the nanotubes in gondola-like structures. (A) Gondola-like structures appear within 10 min after cell seeding. (B) Nanotubes may carry gondolas in varying frequency. Scale bars in A and B represent 800 nm and 5 μm, respectively.

between pillars where they could not easily move (Fig. 7A). The contact these cells formed to the pillars were close, that is, in the nanometer range. This is of great importance when this culture system is intended for use with multielectrode arrays. The distance between conductive surface and cells is essentially influencing the "quality" of the signals transmitted via the metal surface or taken up by it in case of electrically active cells such as neurons. Fromherz [42] reported a distance of 109 nm for astrocytes attached to a silicon chip, 50 nm for fibroblasts attached to the silicon chip by focal contacts and 1 nm for pure phospholipids. The large distance in between astrocytes and silicon chips is assumed to be caused by macromolecules dangling from the glycocalyx of the cell. The very low distance (<2 nm) we observed in TEM images (Fig. 8), suggests that the membranes of nanotubes from astrocytes consist of pure phospholipids, at least on

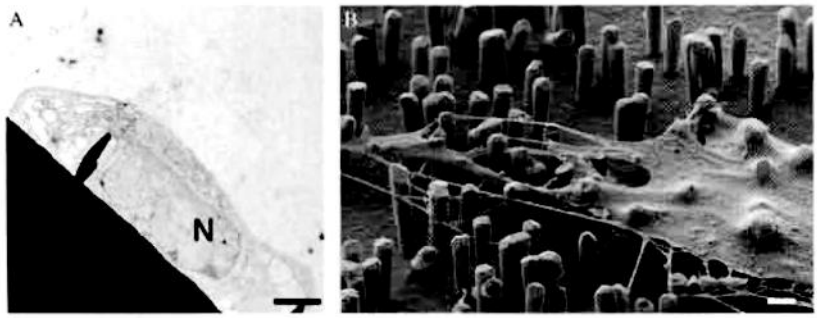

Fig. 7. (A,B). TEM images show that cell bodies and nuclei (marked by "N") were found in between metal pillars while nanotubular protrusions as well as peripheral membrane parts seem to be restricted to the upper parts of the pillars as revealed by SEM images taken at an angle of 45 . Scale bars in A and B represent 2 and 1 μm, respectively.

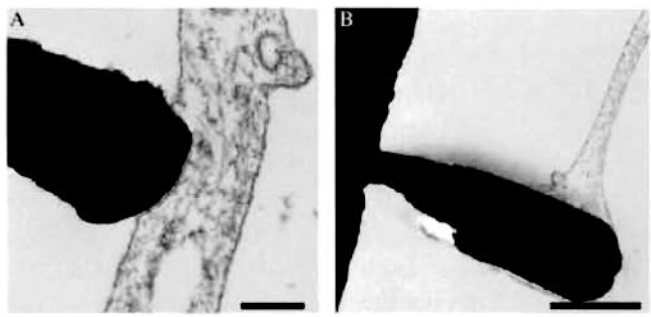

Fig. 8. TEM images show that astrocytes make very close contact to the pillars. The distance is less than 2 nm (measured by TEM at higher magnification). Scale bars in A and B represent 200 nm and 1 μm, respectively.

their tips. This is in line with the already described findings of lipid rafts on the tip of nanotubular protrusions from B cells [24].

One could speculate that the bulb-like contact, formed between astrocytic nanotubes (Fig. 9) and nanolawn pillars, resembles those seen between astrocytic processes and neurons [43]. TEM studies on brain tissue indeed showed that astrocytes surround synapses partially, in order to take up excess glutamate [31].

[2]. We examined whether this mechanism applied to our system, too. To this end, we treated the cells with , which is known to prevent both polymerization [2]. For latrunculin-B treatment, cells were seeded as before onto nanolawns and incubated in medium containing 5 or 10 μM latrunculin B (Calbiochem/Merck, Darmstadt, Germany). The cells were fixed after 1 or 24 h. Surprisingly, the formation of nanotubes was not affected by 5 (Fig. 10B) and 10 μM (Fig. 10C) latrunculin B compared to

Fig. 9. SEM image shows that nanotubes end on pillars in a bulb-like contact. Scale bar = 2 μm.

control cells 1 h after cell seeding (Fig. 10A). The same was true for cells cultured for 24 h in the presence of latrunculin B (Figs. 10D–F).

In addition, the effect of actin depolymerization was checked by exchanging control medium by medium containing latrunculin B after culturing periods of 1 or 23 h. These cultures were fixed an hour later. Here, the stability of nanotubes was not compromised by treatment with 5 (Fig. 11B) and 10 μM (Fig. 11C) latrunculin B compared to control cells 2 h after cell seeding (Fig. 11A). In the latter experiments, latrunculin B was added for 1 h after the cells were allowed to settle for 1 h (Fig. 11B, C). However, it was apparent that latrunculin B was active as we found an overall diminished stability of the cells at 10 μM latrunculin B as even the membranous parts of the cells seemed to sink in between the metal pillars (Fig. 11C). These findings suggest that actin fibers do not play a major role in nanotube formation or stability. This is in line with the already discussed hypothesis of Önfelt *et al.* [7], that nanotubes are constructed from fluid membrane and findings from Karlsson *et al.* [18,19] and our laboratories (see later), that nanotubes and gondolas can be formed in pure phospholipid systems.

Interestingly, we found branched nanotubes forming nets of tubes expanding between cells (Fig. 12A, B). These branched nanotube networks could indicate a special growth pattern or a pattern of what cells leave behind when they retreat as they do when they round up and die. Indeed, we never found them in very fresh cultures (e.g., 2 h) but in cultures >24 h in which we also found empty cell skeletons (Fig. 12C). Thus, we assume it more likely that the branched tubular networks are leftovers of highly interconnected cells which have undergone apoptosis.

Because the nanotubes formed under the influence of latrunculin B did not display regular net branching, as seen in Fig. 12, we assume them not to be traces left behind by moving or dying cells. Another supporting argument for our view that actin [44] or a permanent pulling force [45] are not essential for the formation and stability of nanotubes comes from pure phospholipid systems

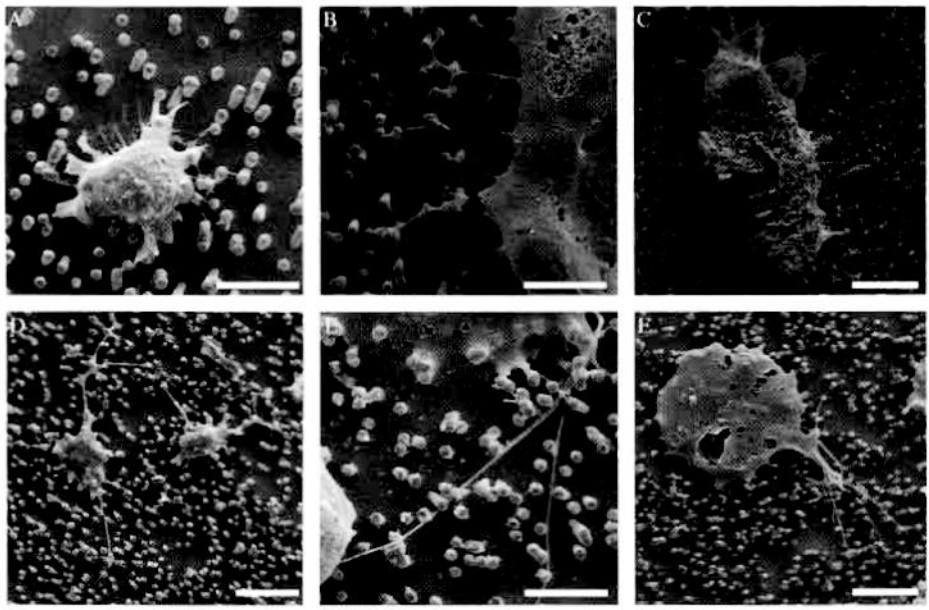

Fig. 10. The formation and stability of nanotubes is not affected by latrunculin B. Astrocytes were cultured in the absence or presence of latrunculin B for 1 h (A–C) or 24 h (D–F). Control (A, D); 5 μM Latrunculin B (B, E); 10 μM Latrunculin B (C, F). Scale bars in A–F represent 5, 5, 10, 10, 5, and 10 μm, respectively.

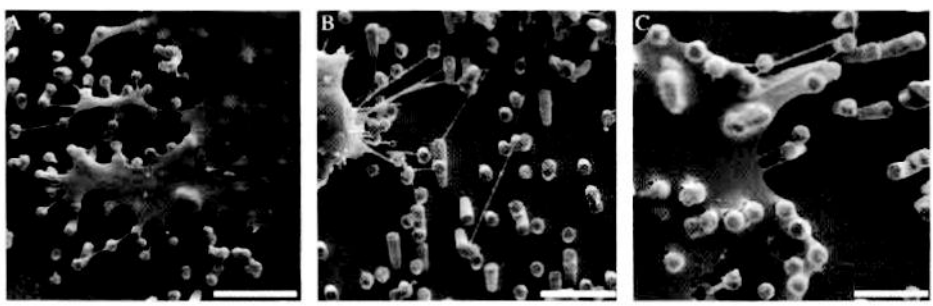

Fig. 11. (A) Control cultures of astrocytes after 2 h on nanolawns. To test the stability of nanotubes in the absence of actin, astrocytes were seeded onto nanolawns for 1 h before addition of (B) 5 and (C) 10 μM latrunculin B for another hour. Scale bars in A, B, C represent 5, 4, and 3 μm, respectively.

(see later) where stable nanotubes have been observed [46–48]. Nevertheless, that actin is not necessary for the formation of tubes does not exclude some supportive role of fiber formation inside the tubes [49,50]. Glial fibrillary acidic protein (GFAP) is a unique marker of astrocytes. We cannot exclude the possibility that astrocytes may utilize an actin-independent cytoskeleton formed by GFAP. Indeed, astrocytes are coupled via thin processes *in vivo* and *in vitro* [51].

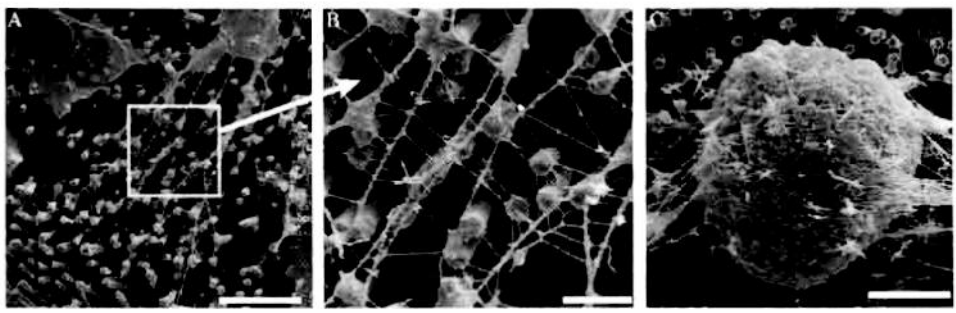

Fig. 12. (A–B) Branched nanotubes forming nets of tubes expanding between cells at different magnifications. (C) In the same culture, empty cell skeletons were found suggesting that branched nanotubes might not occur when cells colonize nanostructures but rather reflect leftovers of cells having retreated from nanotubes to finally die. Scale bars in A, B and C represent 8, 2 and 5 μm, respectively.

Apparently, these processes contain GFAP suggesting that GFAP could be a structural component in process formation [51].

3.3. Thin tubular structures formed by erythrocyte membranes

The results of some recent studies indicated that thin tubular membraneous structures are common also to other cell types, for example, erythrocytes and neuroblasts [2,52]. Nevertheless, they have not been extensively explored in the past because of the experimental difficulties in investigating these thin and fragile structures.

Our observations revealed that tubular budding can be induced by adding amphiphilic detergents (dodecylmaltoside) to erythrocyte suspensions (Fig. 13). Chiral patterns of the intramembraneous particles (IMP) were found neither on the cylindrical buds nor on the released tubular nanoexovesicles. We have shown that the observed amphiphile-induced tubular budding can be theoretically explained by in-plane orientational ordering [48,53] and accumulation of anisotropic membrane inclusions in the budding region. In contrast to some previously reported theories, no mechanical pulling force is needed to explain membrane tubulation [54]. A bilayer-couple mechanism mediated by a conformational shape change of the band 3 membrane protein has been proposed by us as an extremely fast mechanism of shape transition and spike generation in red cells [55]. This mechanism does not require the participation of cytoskeleton elements. Experimental evidence comes from atomic force microscopy images of the spatial need of the band 3 protein [56].

In line with our theoretical prediction it was recently shown that plasma membrane protrusions (microvilli, filopodia, microspikes) exhibit a specific membrane

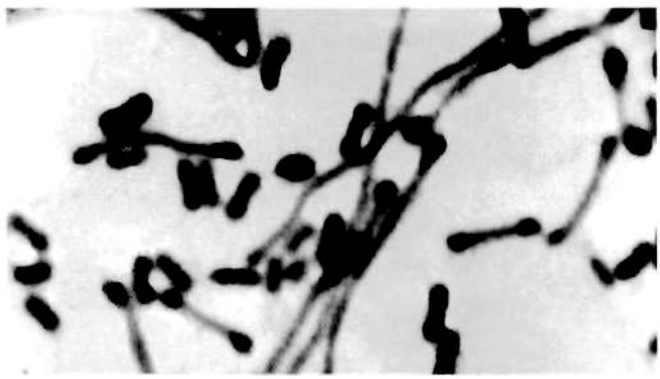

Fig. 13. Micrograph of free nanotubes detached from the surface of the erythrocyte membrane. The formation of membrane nanotubes was induced by adding 40 μM of dodecylmaltoside to the erythrocyte suspension (adapted from [53]). The diameter of the nanotubes is around 40 nm.

protein and lipid composition and organization which differs from that of the planar region of the plasma membrane [57]. Based on the theoretical considerations, it was suggested that the reported concentration of prominin rafts in thin tubular membrane protrusions may be caused by a curvature-induced accumulation of small prominin-lipid complexes (inclusions) in protrusions and their coalescence into larger rafts.

In accordance with this suggestion, we observed persistence of long tubular membrane protrusions devoid of internal rod-like microtubular structure in cells [50]. We suggested that the stability of the tubular membrane protrusions without the inner supporting rod-like cytoskeleton is a consequence of the accumulation of anisotropic membrane inclusions (Fig. 14) in the bilayer membrane of these protrusions.

The theoretically predicted anisotropy-induced lateral phase separation of membrane inclusions may appear also without direct nearest-neighbour interactions [50]. On the other hand, the nearest-neighbour interactions alone may cause lateral phase separation if strong enough. Because a specific prominin raft formation has been indicated only on highly curved tubular membrane protrusions, we assumed that the anisotropy of prominin inclusions is the primary cause of their accumulation in thin tubular membrane protrusions while direct interactions are a secondary effect.

3.4. Nanotube formation in phospholipid systems

Clustering of membrane components into larger domains in highly curved spherical regions (invaginations) of cell membranes has been indicated in multicomponent lipid bilayer systems [58]. Stable thin tubular membrane protrusions have

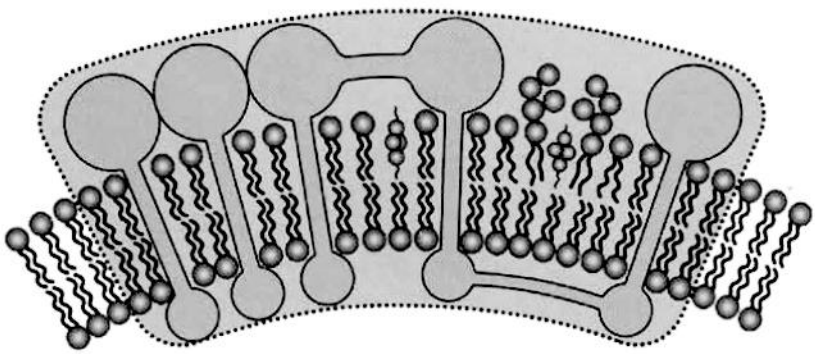

Fig. 14. Schematical figure of a possible structure of a flexible anisotropic membrane inclusion.

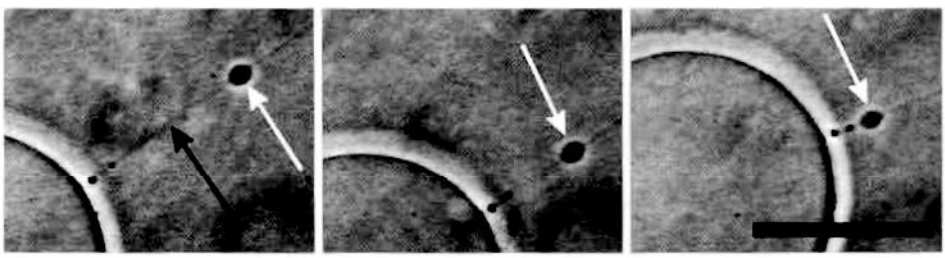

Fig. 15. Movement of a small phospholipid prolate carrier vesicle (white arrow) along a thin phospholipid tube (black arrow) attached to a giant phospholipid vesicle (adapted from [52]). Scale bar = 10 μm.

been observed in one-component giant lipid vesicles (Fig. 15). A simple mechanism, which considers that phospholipid molecules are intrinsically anisotropic, was proposed in order to explain the stability of these protrusions [48]. While the collective effect on almost flat lipid bilayer regions yields the state of a laterally isotropic two-dimensional liquid, the anisotropic properties of lipid molecules express if the lipid bilayer for some reason develops regions of highly different principal curvatures. This mechanism may explain the stability of the phospholipid micro- and nanotubes attached to giant phospholipid vesicles [48] and phospholipid-vesicle shapes that involve narrow necks connecting two spherical vesicles [59].

Based on the earlier described experimental and theoretical results, we suggest that membrane-skeleton detached, laterally mobile membrane components and inclusions may self-assemble into highly curved tubular or spherical membrane protrusions depending on their intrinsic shape and/or direct interactions between them [50,53,60].

3.5. Theoretical discussion

Here we suggest a possible mechanism that may explain the observed self-assembly of tubular membrane protrusions (nanotubes) of astrocytes where the actin fibers are not necessary for the formation of these structures. The complementary mechanism we propose accounts for the formation and stabilization of the observed long tubular membrane protrusions [48,53]. It is based on the energetically favorable orientational ordering [48] and accumulation of membrane inclusions (Fig. 14) on tubular protrusions [50,53] and their self-assembly because of direct interactions and curvature-induced lateral phase separation [50,53]. The membrane inclusion (also called nanoraft) is defined as a very small membrane domain composed of different membrane components [50,53]. The size of the membrane inclusion may correspond to a small number of molecules (Fig. 14).

In the theory, the membrane shape is described as a two-dimensional surface characterized by two invariants of the matrix representing the curvature tensor of the membrane surface: the mean curvature $H = (C_1 + C_2)/2$ and the curvature deviator $D = |C_1 - C_2|/2$, where C_1 and C_2 are the principal membrane curvatures. To calculate the membrane free energy, the membrane is described as a continuum with embedded laterally and rotationally mobile inclusions. Similarly, as the intrinsic shape of single membrane components [60] also, the intrinsic shape of membrane inclusions are characterized by their mean curvature H_m and intrinsic curvature deviator D_m [50,53]. H_m and D_m represent the membrane curvatures that correspond to the minimal possible energy of the membrane inclusion. Inclusions with D_m equal to zero are isotropic while inclusions for D_m differing from zero are anisotropic with respect to the normal axis perpendicular to the membrane (Fig. 16). Nevertheless, not all inclusions in the membrane can attain the minimal energy state. The mismatch between the inclusion shape and the local curvature field reflects the energy of each single inclusion.

For anisotropic inclusions, different orientations with respect to the local principal axes of the membrane yield different single-inclusion energies [48,53]. Therefore, it must be expected that on average an inclusion spends more time in energetically more favorable orientational states. It follows that anisotropic inclusions undergo weak orientational ordering with a stronger effect for larger curvature deviators of the membrane and the inclusion [50]. Upon statistical averaging over all possible orientations of the inclusion, the free energy of the single inclusion can be written in the form [48,50]:

$$f = \frac{\xi}{2}(H - H_m)^2 + \frac{\xi}{2}\left(D^2 + D_m^2\right) - kT \ \ln\left(I_0\left(\frac{\xi D_m D}{kT}\right)\right), \qquad (1)$$

where ξ is the constant, I_0 the modified Bessel function, k the Boltzmann constant and T the absolute temperature.

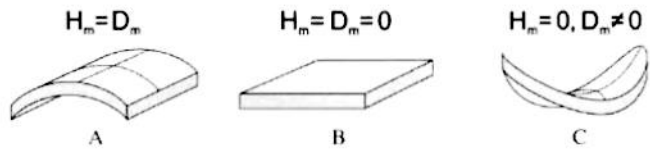

Fig. 16. Schematic figure of the most favorable shapes of flexible membrane inclusions having different values of the intrinsic (spontaneous) mean curvature H_m and intrinsic (spontaneous) curvature deviator D_m: the favorable shape of the membrane inclusion may be characterized by $H_m = D_m > 0$ (A), $H_m = D_m = 0$ (B) and $H_m = 0$ and $D_m \neq 0$ (C).

Inclusions in aggregates interact with neighbouring inclusions. We denote the corresponding interaction energy per inclusion (monomer) in the aggregate composed of i inclusions $\chi(i)$ and assume that $\chi(i)$ depends on the size of the aggregate i. Hence, the mean energy per inclusion in the cylindrical aggregate composed of i inclusions can be written as $\mu_i = f_c - \chi(i)$, where $f_c = f(H = D)$ and $\chi(i) > 0$. We further assume that in the planar regions of the membrane (having $H = D = 0$), the concentration of inclusions is always below the critical aggregation concentration (CAC) [for definition of CAC see: Ref. 61]. Therefore, the inclusion cannot form two-dimensional flat aggregates and the mean energy per inclusion in the flat membrane regions is $\tilde{\mu}_i = f_p$, where $f_p = f(H = D = 0)$.

The concentration (mole fraction) of the inclusions in the flat membrane regions is $\tilde{x}_1 = \tilde{N}_1 / M$, where $\tilde{N}_1$ is the number of monomer-inclusions in flat regions and M is the number of (lattice) sites in the whole system. The size distribution of cylindrical aggregates on the concentrations scale is $x_i = iN_i/M$, where N_i denotes the number of cylindrical aggregates with aggregation number i, that is, the number of tubular membrane protrusions (N_i) each consisting of i inclusions. The concentrations $\tilde{x}_1$ and x_i should fulfill the conservation conditions for the total number of inclusions in the membrane: $\tilde{x}_1 + \sum_{i=1}^{\infty} x_i = N/M$. The free energy of all inclusions in the membrane is composed of the energies of the monomer inclusions, the energies of all inclusion aggregates, the mixing entropy of the monomer inclusions and the mixing entropy of all inclusion aggregates. Aggregates of the same size are treated as equal and indistinguishable. Using the Lagrange method, the minimization of the function:

$$f = M\left[\tilde{x}_1\tilde{\mu}_1 + kT\tilde{x}_1(\ln \tilde{x}_1 - 1)\right] + M\sum_{i=1}^{\infty}\left[x_i\mu_i + kT\frac{x_i}{i}\left(\ln\frac{x_i}{i} - 1\right)\right] - \mu M\left(\tilde{x}_1 + \sum_{i=1}^{\infty} x_i\right) \tag{2}$$

with respect to $\tilde{x}_1$ and x_i, leads to equilibrium distributions:

$$\tilde{x}_1 = \exp\left(\frac{f_p - \mu}{kT}\right) \tag{3}$$

$$x_i = i\exp\left(-\frac{i}{kT}[f_c - \chi - \mu]\right) \tag{4}$$

where μ is the Lagrange parameter. For simplicity, we assumed $\chi(i)$ to be constant. The quantity μ can be derived from equation (3) and inserted in equation (4) to get:

$$x_i = i\left[\tilde{x}_i \cdot \exp\left(\frac{f_p + \chi - f_c}{kT}\right)\right]. \tag{5}$$

Since x_i cannot exceed unity, from equation (5) follows that when $\tilde{x}_1$approaches $\exp((f_c - f_p - \chi)/kT)$, it cannot be increased further. The maximal possible value of concentration of monomeric inclusions in flat parts of the membrane $\tilde{x}_1$ is therefore:

$$\tilde{x}_c \approx \exp\left(\frac{\Delta f - \chi}{kT}\right), \tag{6}$$

where $\Delta f = f_c - f_p$ is the difference between the energy of the single inclusion on the cylindrical protrusion and its energy of the inclusion in the flat membrane region. The concentration $\tilde{x}_c$ is the CAC [61,62]. In the case of cylindrical aggregates, where $H = D = 1/2r$ from equation (1) follows:

$$\Delta f = \xi H(H - H_m) - kT\ln\left[I_0(\xi D_m D/kT)\right]. \tag{7}$$

For $1/2r < H_m$, the value of Δf is always negative. If $\tilde{x}_1$ is above $\tilde{x}_c$, the formation of very long cylindrical protrusions with assembled anisotropic inclusions is promoted. This effect is additionally enhanced if the concentration of the monomers in the flat part is above critical. The minimization of the membrane free energy also yields the equilibrium radius of the tubular protrusion which depends on the intrinsic curvatures of the inclusions and their concentration in the membrane.

Within tubular parts, anisotropic inclusions undergo orientational ordering and therefore represent regions of higher order within the membrane. This can be interpreted as rafts formed on the tubular parts that are consistently related to the stable tubular shape with a particular equilibrium radius. However, concentration of monomers in the tubular part is higher than in the flat parts already when the monomer concentrations in flat parts are below the critical concentration ($x_1 \gg \tilde{x}_1$ also for $\tilde{x}_1 < \tilde{x_c}$), indicating that anisotropic membrane inclusions may play an important role in generation and stabilization of thin tubular membrane protrusions even below the CAC. Equations (6–7) show that the longitudinal growth of cylindrical membrane protrusions is promoted by the energy difference Δf as well as by the strength of the direct interactions between the inclusions χ. The critical concentration $\tilde{x}_c$ strongly decreases with increasing D_m.

4. CONCLUSIONS

Nanotubular structures can not only be found in many cell types but also in pure phospholipid systems, that is, liposomes. They are involved in cellular communication, material transport and signal transduction. While actin has been found in nanotubes extended by cells, it may not always be necessary for the formation of nanotubes. Our experimental data show that actin is not required for formation and stability of nanotubes. This view is supported by experimental evidence. Our theoretical considerations suggest a new model of nanotube formation without actin involved.

ACKNOWLEDGMENTS

The authors thank the staff of the electron microscopy center at the University of Rostock's Medical Faculty for outstanding technical support. C. Voigt is acknowledged for excellent technical assistance. The authors are grateful to B. Babnik for help with preparation of the figures. This study has been supported by grants 01 ZZ 0108 from the Bundesministerium für Bildung und Forschung (Federal Ministry for Education and Research) and the Hertie Foundation (1.01.1/03/014) to U.G. and StSch 2002 0418A from the Bundesamt für Strahlenschutz (Federal Office for Radiation Protection) to J.G.. S.F. and M.Z. have been financed by IZM intramural funding. The silicon neurochip experiments were conducted by W. Baumann, C. Tautorat and A. Podssun and sponsored by the European Regional Development Fund (ERDF), the state Mecklenburg-Western Pomerania and Micronas GmbH. The German Academic Exchange Service (DAAD) fellowship supporting the stay of A.I. at the University of Rostock is gratefully acknowledged.

REFERENCES

[1] H. Gerhardt, M. Golding, M. Fruttiger, C. Ruhrberg, A. Lundkvist, A. Abramsson, M. Jeltsch, C. Mitchell, K. Alitalo, D. Shima, C. Betsholtz, VEGF guides angiogenic sprouting utilizing endothelial tip cell filopodia, J. Cell Biol. 161 (2003) 1163–1177.
[2] A. Rustom, R. Saffrich, I. Markovic, P. Walther, H.H. Gerdes, Nanotubular highways for intercellular organelle transport, Science 303 (2004) 1007–1010.
[3] D. Zhu, K.S. Tan, X. Zhang, A.Y. Sun, G.Y. Sun, J.C. Lee, Hydrogen peroxide alters membrane and cytoskeleton properties and increases intercellular connections in astrocytes, J. Cell Sci. 118 (2005) 3695–3703.
[4] G. Morata, K. Basler, Cells in search of a signal, Nat. Cell Biol. 1 (1999) E60–E61.
[5] F.A. Ramirez-Weber, T.B. Kornberg, Cytonemes: cellular processes that project to the principal signaling center in Drosophila imaginal discs, Cell. 97 (1999) 599–607.
[6] D. Cuvelier, I. Derenyi, P. Bassereau, P. Nassoy, Coalescence of membrane tethers: experiments, theory, and applications, Biophys. J. 88 (2005) 2714–2726.
[7] B. Önfelt, S. Nedvetzki, K. Yanagi, D.M. Davis, Cutting edge: membrane nanotubes connect immune cells, J. Immunol. 173 (2004) 1511–1513.

[8] T. Gustafson, L. Wolpert, Studies on the cellular basis of morphogenesis in the sea urchin embryo. Directed movements of primary mesenchyme cells in normal and vegetalized larvae, Exp. Cell Res. 24 (1961) 64–79.
[9] W. Wood, P. Martin, Structures in focus—filopodia, Int. J. Biochem. Cell Biol. 34 (2002) 726–730.
[10] M.J. Dalby, C.C. Berry, M.O. Riehle, D.S. Sutherland, H. Agheli, A.S. Curtis, Attempted endocytosis of nano-environment produced by colloidal lithography by human fibroblasts, Exp. Cell Res. 295 (2004) 387–394.
[11] A.J. Zhu, M.P. Scott, Incredible journey: how do developmental signals travel through tissue? Genes Dev. 18 (2004) 2985–2997.
[12] S.C. Watkins, R.D. Salter, Functional connectivity between immune cells mediated by tunneling nanotubules, Immunity 23 (2005) 309–318.
[13] J.L. Spees, S.D. Olson, M.J. Whitney, D.J. Prockop, Mitochondrial transfer between cells can rescue aerobic respiration, Proc. Natl. Acad. Sci. USA 103 (2006) 1283–1288.
[14] J.R. Robbins, A.I. Barth, H. Marquis, E.L. de Hostos, W.J. Nelson, J.A. Theriot, Listeria monocytogenes exploits normal host cell processes to spread from cell to cell, J. Cell Biol. 146 (1999) 1333–1350.
[15] A.J. Merz, H.N. Higgs, Listeria motility: biophysics pushes things forward, Curr. Biol. 13 (2003) R302–R304.
[16] M.M. Stevens, J.H. George, Exploring and engineering the cell surface interface, Science 310 (2005) 1135–1138.
[17] M.J. Dalby, M.O. Riehle, H.J. Johnstone, S. Affrossman, A.S. Curtis, Nonadhesive nanotopography: fibroblast response to poly(n-butyl methacrylate)-poly(styrene) demixed surface features, J. Biomed. Mater. Res. A. 67 (2003) 1025–1032.
[18] M. Karlsson, K. Sott, M. Davidson, A.S. Cans, P. Linderholm, D. Chiu, O. Orwar, Formation of geometrically complex lipid nanotube-vesicle networks of higher-order topologies, Proc. Natl. Acad. Sci. USA. 99 (2002) 11573–11578.
[19] A. Karlsson, R. Karlsson, M. Karlsson, A.S. Cans, A. Stromberg, F. Ryttsen, O. Orwar, Networks of nanotubes and containers, Nature 409 (2001) 150–152.
[20] A.S. Cans, N. Wittenberg, R. Karlsson, L. Sombers, M. Karlsson, O. Orwar, A. Ewing, Artificial cells: unique insights into exocytosis using liposomes and lipid nanotubes, Proc. Natl. Acad. Sci. USA 100 (2003) 400–404.
[21] R.D. Salter, R.J. Tuma-Warrino, P.Q. Hu, S.C. Watkins, Rapid and extensive membrane reorganization by dendritic cells following exposure to bacteria revealed by high-resolution imaging, J. Leukoc. Biol. 75 (2004) 240–243.
[22] J.H. Niess, S. Brand, X. Gu, L. Landsman, S. Jung, B.A. McCormick, J.M. Vyas, M. Boes, H.L. Ploegh, J.G. Fox, D.R. Littman, H.C. Reinecker, CX3CR1-mediated dendritic cell access to the intestinal lumen and bacterial clearance, Science 307 (2005) 254–258.
[23] S.I. Galkina, G.F. Sud'ina, V. Ullrich, Inhibition of neutrophil spreading during adhesion to fibronectin reveals formation of long tubulovesicular cell extensions (cytonemes), Exp. Cell Res. 266 (2001) 222–228.
[24] N. Gupta, A.L. DeFranco, Visualizing lipid raft dynamics and early signaling events during antigen receptor-mediated B-lymphocyte activation, Mol. Biol. Cell. 14 (2003) 432–444.
[25] D.M. Davis, M.L. Dustin, What is the importance of the immunological synapse? Trends Immunol. 25 (2004) 323–327.
[26] S.I. Galkina, J.G. Molotkovsky, V. Ullrich, G.F. Sud'ina, Scanning electron microscopy study of neutrophil membrane tubulovesicular extensions (cytonemes) and their role in anchoring, aggregation and phagocytosis. The effect of nitric oxide, Exp. Cell Res. 304 (2005) 620–629.
[27] F.Q. Zhou, C.S. Cohan, How actin filaments and microtubules steer growth cones to their targets, J. Neurobiol. 58 (2004) 84–91.
[28] E. Hansson, L. Ronnback, Astrocytes in glutamate neurotransmission, FASEB J. 9 (1995) 343–350.

[29] W. Walz, Role of astrocytes in the clearance of excess extracellular potassium, Neurochem. Int. 36 (2000) 291–300.
[30] J. Grosche, V. Matyash, T. Moller, A. Verkhratsky, A. Reichenbach, H. Kettenmann, Microdomains for neuron-glia interaction: parallel fiber signaling to Bergmann glial cells, Nat. Neurosci. 2 (1999) 139–143.
[31] R. Ventura, K.M. Harris, Three-dimensional relationships between hippocampal synapses and astrocytes, J. Neurosci. 19 (1999) 6897–6906.
[32] J. Hirrlinger, S. Hulsmann, F. Kirchhoff, Astroglial processes show spontaneous motility at active synaptic terminals in situ, Eur. J. Neurosci. 20 (2004) 2235–2239.
[33] J.L. Ridet, S.K. Malhotra, A. Privat, F.H. Gage, Reactive astrocytes: cellular and molecular cues to biological function, Trends Neurosci. 20 (1997) 570–577.
[34] A. Verkhratsky, R.K. Orkand, H. Kettenmann, Glial calcium: homeostasis and signaling function, Physiol Rev. 78 (1998) 99–141.
[35] K.P. Lehre, N.C. Danbolt, The number of glutamate transporter subtype molecules at glutamatergic synapses: chemical and stereological quantification in young adult rat brain, J. Neurosci. 18 (1998) 8751–8757.
[36] F. Luthen, R. Lange, P. Becker, J. Rychly, U. Beck, J.G. Nebe, The influence of surface roughness of titanium on beta1- and beta3-integrin adhesion and the organization of fibronectin in human osteoblastic cells, Biomaterials 26 (2005) 2423–2440.
[37] S.A. Catledge, M.D. Fries, Y.K. Vohra, W.R. Lacefield, J.E. Lemons, S. Woodard, R. Venugopalan, Nanostructured ceramics for biomedical implants, J. Nanosci. Nanotechnol. 2 (2002) 293–312.
[38] A.M. Turner, N. Dowell, S.W. Turner, L. Kam, M. Isaacson, J.N. Turner, H.G. Craighead, W. Shain, Attachment of astroglial cells to microfabricated pillar arrays of different geometries, J. Biomed. Mater. Res. 51 (2000) 430–441.
[39] G. Krause, S. Lehmann, M. Lehmann, I. Freund, E. Schreiber, W. Baumann, Measurement of electrical activity of long-term mammalian neuronal networks on semiconductor neurosensor chips and comparison with conventional microelectrode arrays, Biosens. Bioelectron. 21 (2006) 1272–1282.
[40] C. Schönenberger, B.M.I. van der Zande, L.G.J. Fokkink, M. Henny, C. Schmid, M. Krüger, A. Bachtold, R. Huber, H. Birk, U. Staufer, Template Synthesis of Nanowires in Porous Polycarbonate Membranes: Electrochemistry and Morphology, J. Phys. Chem. B 101 (1997) 4597–5505.
[41] U. Gimsa, A. Oren, P. Pandiyan, D. Teichmann, I. Bechmann, R. Nitsch, M.C. Brunner-Weinzierl, Astrocytes protect the CNS: antigen-specific T helper cell responses are inhibited by astrocyte-induced upregulation of CTLA-4 (CD152), J. Mol. Med. 82 (2004) 364–372.
[42] P. Fromherz, in:R. Waser (Ed.), Nanoelectronics and Information Technology, Wiley-VCH, Berlin, 2003, pp. 781, 810
[43] L. Duan, H. Yuan, C.J. Su, Y.Y. Liu, Z.R. Rao, Ultrastructure of junction areas between neurons and astrocytes in rat supraoptic nuclei, World J. Gastroenterol. 10 (2004) 117–121.
[44] H. Miyata, S. Nishiyama, K. Akashi, K. Kinosita Jr., Protrusive growth from giant liposomes driven by actin polymerization, Proc. Natl. Acad. Sci. USA 96 (1999) 2048–2053.
[45] M. Sun, J.S. Graham, B. Hegedus, F. Marga, Y. Zhang, G. Forgacs, M. Grandbois, Multiple membrane tethers probed by atomic force microscopy, Biophys. J. 89 (2005) 4320–4329.
[46] L. Mathivet, S. Cribier, P.F. Devaux, Shape change and physical properties of giant phospholipid vesicles prepared in the presence of an AC electric field, Biophys. J. 70 (1996) 1112–1121.
[47] V. Kralj-Iglič, G. Gomišček, J. Majhenc, V. Arrigler, S. Svetina, Myelin-like protrusions of giant phospholipid vesicles prepared by electroformation, Colloids Surf. A 181 (2001) 315–318.

[48] V. Kralj-Iglič, A. Iglič, G. Gomišček, V. Arrigler, H. Hägerstrand, Microtubes and nanotubes of phospholipid bilayer vesicles, J. Phys. A. Math. Gen. 35 (2002) 1533–1549.
[49] D. Corbeil, K. Roper, C.A. Fargeas, A. Joester, W.B. Huttner, Prominin: a story of cholesterol, plasma membrane protrusions and human pathology, Traffic 2 (2001) 82–91.
[50] A. Iglič, H. Hägerstrand, P. Veranič, A. Plemenitaš, V. Kralj-Iglič, Curvature-induced accumulation of anisotropic membrane components and raft formation in cylindrical membrane protrusions, J. Theor. Biol. 240 (2006) 368–373.
[51] N. Duval, D. Gomes, V. Calaora, A. Calabrese, P. Meda, R. Bruzzone, Cell coupling and Cx43 expression in embryonic mouse neural progenitor cells, J. Cell Sci. 115 (2002) 3241–3251.
[52] A. Iglič, H. Hägerstrand, M. Bobrowska-Hägerstrand, V. Arrigler, V. Kralj-Iglič, Possible role of phospholipid nanotubes in directed transport of membrane vesicles, Phys. Lett. A 310 (2003) 493–497.
[53] V. Kralj-Iglič, H. Hägerstrand, P. Veranič, K. Jezernik, B. Babnik, D.R. Gauger, A. Iglič, Amphiphile-induced tubular budding of the bilayer membrane, Eur. Biophys. J. 34 (2005) 1066–1070.
[54] I. Derenyi, F. Jülicher, J. Prost, Formation and interaction of membrane tubes, Phys. Rev. Lett. 88 (2002) 238101-01–238101/04.
[55] J. Gimsa, A possible molecular mechanism governing human erythrocyte shape, Biophys. J. 75 (1998) 568–569.
[56] T. Betz, U. Bakowsky, M.R. Muller, C.M. Lehr, I. Bernhardt, Conformational change of membrane proteins leads to shape changes of red blood cells, Bioelectrochemistry in press (2006).
[57] W.B. Huttner, J. Zimmerberg, Implications of lipid microdomains for membrane curvature, budding and fission, Curr. Opin. Cell Biol. 13 (2001) 478–484.
[58] J.M. Holopainen, M.I. Angelova, P.K. Kinnunen, Vectorial budding of vesicles by asymmetrical enzymatic formation of ceramide in giant liposomes, Biophys. J. 78 (2000) 830–838.
[59] V. Kralj-Iglič, B. Babnik, D.R. Gauger, S. May, A. Iglič, Quadrupolar ordering of phospholipid molecules in narrow necks of phospholipid vesicles, J. Stat. Phys. 121 (in press) (2006).
[60] H. Hägerstrand, L. Mrowczynska, R. Salzer, R. Prohaska, K.A. Michelsen, V. Kralj-Iglič, A. Iglič, Curvature dependent lateral distribution of raft markers in the human erythrocyte membrane, Mol. Membr. Biol. 23 (2006) 277–288.
[61] J.N. Israelachvili, Intermolecular and Surface Forces, Academic Press, London, 1997.
[62] K. Bohinc, A. Iglic, S. May, Self-assembly of linear aggregates on curved membranes, Europhys. Lett. 71 (2005) 145–151.